International Journal of Industrial Engineering and Technology.
ISSN 0974-3146 Volume 18, Number 1 (2026), pp. 63 - 76

http://www.irphouse.com

Optical Properties of $Zn_{1-x}Mn_xS$ Thin Films Prepared by Spray Pyrolysis Technique for Application in Spintronic Devices

Muslima Zahan[1], Krishna Pada Mondal[2], Jiban Podder[3]
[1,2]University of Information Technology and Sciences, Bangladesh
[3]University of Saskatchewan, Canada
Corresponding Author's Email: muslimazahan30@gmail.com

Abstract
In the present study, Mn doped ZnS ($Zn_{1-x}Mn_xS$, where, x = 0.1, 0.3, 0.5 and0.7 M;) thin films have been deposited onto glass substrates at 823 K substrate temperature using a spray pyrolysis deposition technique to explore the effect of Mn into the ZnS matrix for spintronic devices application. Field emission scanning electron microscopy (FESEM) indicates the homogeneous and smooth crystalline surface of $Zn_{1-x}Mn_xS$ thin films and have been suggested the increased grain size with an increase in Mn concentration. Energy Dispersive X-ray (EDAX) spectra confirms the presence of Mn^{2+} in ZnS films. The UV–visible absorption spectra of $Zn_{1-x}Mn_xS$ thin films have been taken in the wavelength range 200–1100 nm and observed the transparent films with small absorption in the visible region. The absorption peaks show redshift with the addition of Mn. The optical band gaps are found to be red-shifted from 3.45 to 3.05 eV due to the increase in the crystalline nature of the thin films. The other optical parameters such as reflectance, extinction coefficient, refractive index and dielectric constant indicate the good crystalline nature of the $Zn_{1-x}Mn_xS$ thin films which can be suitable in spintronic devices.

Keywords: $Zn_{1-x}Mn_xS$, thin films, FESEM, optical properties, band gap energy

1. Introduction

In the modern technology thin film chalcogenides are extremely desirable and promising in spintronic devices. In advanced scientific area diluted magnetic semiconductor (DMS) thin films have drawn much research attention due to their physical and chemical properties and their wide direct band gap energy [1, 2]. The most common DMS are transition metal (Mn, Fe or Co) doped II-VI binary compounds like CdTe, ZnSe, ZnS, CdSe, CdS, etc Among the family of II–VI binary chalcogenide semiconducting thin films Zinc sulfide (ZnS) is look up a prominent semiconductor thin film due to its unique optical, structural and electrical properties, nontoxicity, inexpensive and having wide direct energy gap of 3.60-3.70 eV [3-5], high refractive index from 2.1 to 2.4 and high transmittance from 51% to over 90% in the visible-NIR region [6-8] To improve device performance of DMS, the transition metals like $In^{3+,}$ $Cd^{2+,}$ Al^{3+} $Cu^{2+,}$ $Ag^{2+,}$ Mn^{2+} and Pb^{2+} etc. are doped in ZnS crystal lattice for tunability of optical band gap and other optical properties, modifying the structural, electrical, and magnetic properties. . Although a great deal of research works have been investigated on semiconductor compound, till date very few research works on

optical and electrical properties of DMS thin films have been carried out for spintronic devices. Manganese (Mn) doped zinc sulfide (ZnS) ; ($Zn_{1-x}Mn_xS$) DMS thin films are one of the most often studied materials [9-11] which have proved to be adequate for spintronic devices application. Since the ionic radius of Mn^{2+} (0.83 Å) is larger than Zn^{2+} (0.74 Å), and the ionic charge is same it can be generally incorporated into different sites of ZnS lattice. The excitation and decay of Mn^{2+} ion produces blue shift and red shift in Vis-NIR region which is highly promising material for spintronic devices. [12-14].

In 2025, Carranza, J., et al. studied optical properties of Mn doped ZnS nanoparticles and found red shift in band gap suitable for Photoluminescence application[15]. In 2024, Ravi, A et al. studied tunable optical band gap of Mn doped ZnS nanoparticles and observed suitability for electro-optic applications [16]. Ali., R, S., et al. studied on Mg-doped ZnS thin films deposited by spray pyrolysis method, in 2023 and observed increased absorption coefficient which suggested that they could be used in photovoltaic applications [17]. In 2022, Aghaei, F., et. Al., studied Cu doped ZnS thin films and found the suitability for application in light emitting diode [18]. Barman, B. et. Al., in 2020 carried out Mn doped ZnS for solar cell applications [19]. However, In spite of having a lot of research works on optical properties of Mn doped ZnS thin films, there is a little attention to explore optical properties of Mn doped ZnS DMS thin films for application in spintronic devices.

Several techniques are used to synthesize DMS thin film such as sol-gel [20], pulsed laser deposition (PLD) [21], atomic layer epitaxy [22], dip-coating technique [23], and spray pyrolysis deposition (SPD) technique [24-26]. Among them, spray pyrolysis deposition method offers interesting possibilities to prepare $Zn_{1-x}Mn_xS$ thin films due to its simplicity, cost-effective, high-quality and nanostructured films deposition parameters. In the present work effect of Mn^{2+} concentration on the spray deposited $Zn_{1-x}Mn_xS$ thin films have been studied to modify optical properties suitable for spintronic devices application.

2. Experimental details

2.1 Precursor materials

The analytical grade Zinc acetated dihydrate [Zn $(CH_3COO)_2.2H_2O$] powder (Mark, Germany 99% purity), manganese (II) acetate tetra-hydrate $Mn(CH_3COO)_2.4H_2O$ powder (Merck, Germany, 99.5% purity) and thiourea (NH_2CSNH_2) were used as mother precursor for Zinc ions (Zn^{2+}), Manganese ions (Mn^{2+}) and sulphide source (S^{2-}) respectively. Deionized distilled water was used as a solvent and ethanol (C_2H_5OH) as stable reagent to control the pH value. Plane glass slides of area 5 × 2.5 cm^2 were used as substrate with a suitable mask. The substrates were soaked with acetone and distilled water in an ultrasonic cleaner for 30 mins and subsequently dried in flowing hot air to execute a better adherence between the film and the substrate.

2.2 Synthesis and processing

In this study Mn doped ZnS thin films were synthesized on plain glass substrate by SPD technique with various Mn concentrations of 0, 1, 3, 5 and 7 at%. In a typical procedure, the working solution was prepared by taking 0.1M Zinc acetated [Zn $(CH_3COO)_2.2H_2O$], 0.1M Manganese acetated [$Mn(CH_3COO)_2.4H_2O$] and 0.2M thiourea (NH_2CSNH_2) dissolving into 100 mL deionized distilled water at room temperature. In solution the concentration ratio of Zinc acetated, Manganese acetated and thiourea were 1:1:2 as thiourea is a slow reactant and synthesis with equimolar ratio was unsuccessful and smaller amounts of thiourea lead to the formation of zinc oxide rather than zinc sulphide. Few drops of ethanol (C_2H_5OH) were included as a stable reagent into the mixture and the mixed

solvent was stirred about 1 hour with a magnetic stirrer to form a homogeneous fuscous slurry. After that, the solution was filtered and then sprayed through a fine bore in the form of fine droplets on pre-heated glass substrates with a deposition time of 25 minutes. The synthesis process of thin films by SPD technique is displayed in Figure-1.

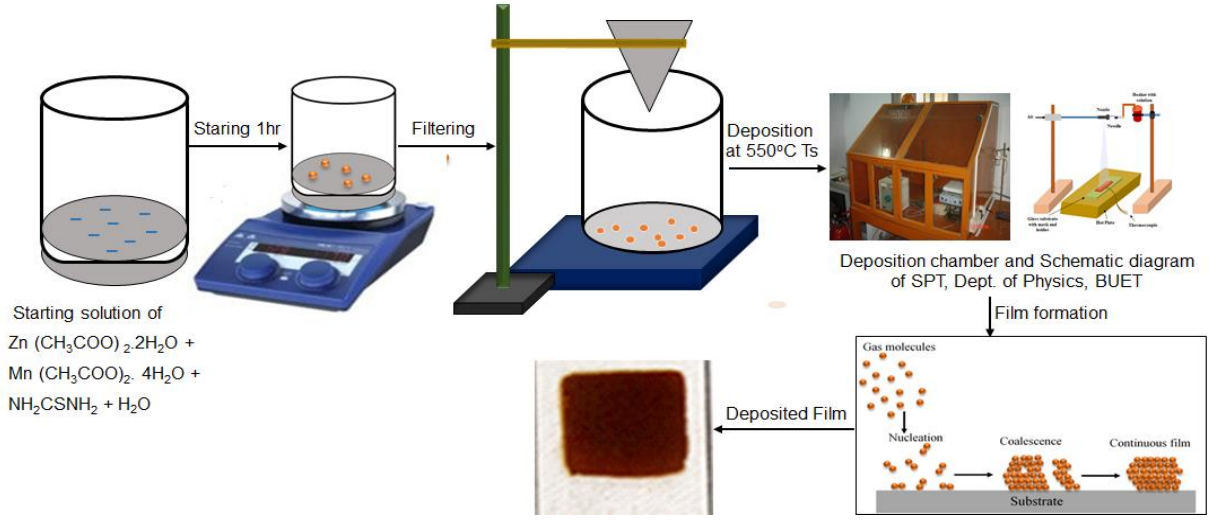

Fig.1. Schematic diagram of $Zn_{1-x}Mn_xS$ thin films synthesis process of by SPD technique

In the system, the temperature of the substrate was kept at 550°C constant. The distance between the spray nozzle and the substrate was kept at 25 cm. The pressure of the carrier gas air was maintained 0.5 bar. The spray rate was maintained at 0.5 mL min^{-1} throughout the experiment. After deposition, the thin films were allowed to cool to room temperature. The as-deposited thin films were found homogeneous and dark brown in color.

Chemical Reaction:

In aqueous solution

$$Zn\,(CH_3COO)_2.2H_2O \xrightarrow{\text{dissociated}} Zn^{2+} + (CH_3COO)^- + H_2O\uparrow$$

$$Mn(CH_3COO)_2.4H_2O \xrightarrow{\text{dissociated}} Mn^{2+} + (CH_3COO)^- + H_2O\uparrow$$

$$NH_2CSNH_2 \xrightarrow{\text{dissociated (H-OH)}} S^{2-} + NH_3\uparrow + CO_2\uparrow + CH_4\uparrow$$

So ZnS nucleate due to the reaction between Zn^{+2} ion and S^{-2} ion as:

$$Zn(CH_3COO)_2.2H_2O + NH_2CSNH_2 \xrightarrow{\text{decomposes at 550°C}} ZnS\downarrow + CH_3COOH + NH_3\uparrow + CO_2\uparrow + CH_4\uparrow$$

Due to different Mn concentration Zn/Mn ratio with NH_2CSNH_2 is considered as:

$$(1\text{-}x)Zn(CH_3COO)_2.2H_2O + (x)Mn(CH_3COO)_2.4H_2O + NH_2CSNH_2 \xrightarrow{\text{deposited at 550°C}} Zn_{1-x}Mn_xS + CH_3COOH + \text{others}$$

2.3 Characterization

The surface morphology of the as-deposited films was studied by field emission scanning electron microscope (FESEM), Model: JSM-7600F operated at 25 kV with an EDAX attached to it. The thickness of the as deposited films was measured by multiple-beam Fizeau fringes method. Optical characterization of the films was carried out over 200–1100 nm wavelength by a UV-1601, Pc: UV–VIS–NIR; Shimadzu, double beam spectrophotometer.

3 Results and discussion

3.1 Surface morphology

Figure-2 displays the FESEM micrographs of the $Zn_{0.7}Mn_{0.3}S$ films with Energy Dispersive X-ray (EDAX) spectra taken at 10,000 magnifications with the scale bar length 10 μm and shows nanostructured polycrystalline surface with 0.2μm average crystallite size. The crystallinity increased with increasing Mn concentration. Because for low Mn concentration, Mn^{+2} ions may be isolated by Zn^{2+} ions and no Mn^{2+} pairs are formed. Due to higher Mn concentration Mn^{2+} ions are incorporated into ZnS lattice and substituted for host cation sites, occurring transition between the s-p electrons of ZnS and d electrons of Mn [27]. The incorporation of Mn^{2+} ions into the lattice of ZnS films greatly affects the morphological feature and porous nature. Figure-3 shows the Energy Dispersive X-ray (EDAX) spectra of the $Zn_{0.7}Mn_{0.3}S$ films. Different peaks corresponding to Zn and S are found in the spectrum, which confirms the ZnS thin film. Sulphur deficiency was observed in all the films shown in Table-1.

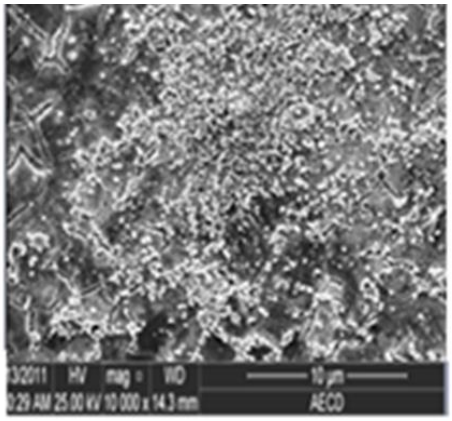

Fig. 2. FESEM image of $Zn_{0.7}Mn_{0.3}S$ film film

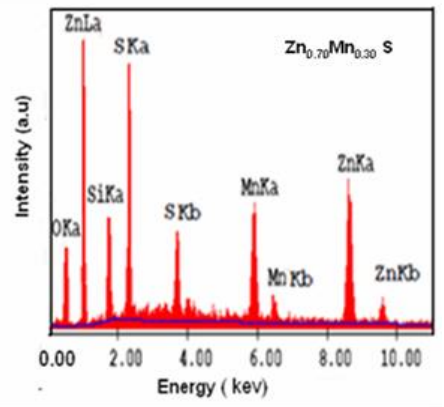

Fig. 3. EDAX spectra of $Zn_{0.7}Mn_{0.3}S$

Table 1 Atomic % of different elements of $Zn_{1-x}Mn_xS$ thin films

At%	Pure ZnS (x = 0.00 mole)	$Zn_{0.90}Mn_{0.10}S$ (x = 0.10 mole)	$Zn_{0.70}Mn_{0.30}S$ (x = 0.30 mole)	$Zn_{0.50}Mn_{0.50}S$ (x=0.50 mole)
Zn	53.17	51.70	48.59	43.93
S	37.12	23.74	15.88	18.17
Mn	0.00	12.82	23.85	28.65
Si	08.49	11.51	07.30	17.10
O	01.22	0.23	04.38	10.15
Total:	100.00	100.00	100.00	100.00

Since Sulphur has great affinity towards oxygen, it is converted to SO_2 and then evaporated. A strong Si peak is observed which corresponds to Si (Substrate) and an Oxygen peak is also observed which is also for substrate. At high operating voltage the electron beam penetrates the film and reaches the glass surface, which results the Si and Oxygen peak. From the table it is observed that the synthesized thin films are stoichiometric. It is also observed that the composition of the thin film does not change due to doping concentration [28].

3.2 Optical transmittance

Figure-4 shows the optical transmittance spectra of $Zn_{1-x}Mn_xS$ (where x = 0.00, 0.05, 0.10, 0.30, 0.50, and 0.70 mole) thin films variation with wavelength in the range of 300 nm to 1100 nm. The optical transmissions of all the films increased with increase in wavelength and are about 80% in the visible region (at 400-600nm) for undoped ZnS film. It is also clearly observed that the transmission decreases with the increase of Mn doping concentration within the 400-600 nm wavelength range. This effect of the Mn doping may for the structural effects. Also, some physical effects such as surface irregularity and defect density may cause the reduction in the transmission. In the IR region (800–1100 nm) transmittance decreases with Mn concentration due to the absorption of light of the excitation electrons from valence band (VB) to conduction band (CB) exhibiting a blue shift into the absorption onset. At 0.3 mole Mn doping concentration transmittance increases which may due to the effects of excess charge carrier of Mn^{2+} ions attributing an improvement of the films in a stoichiometry and may suitable for spintronic devices. [29]

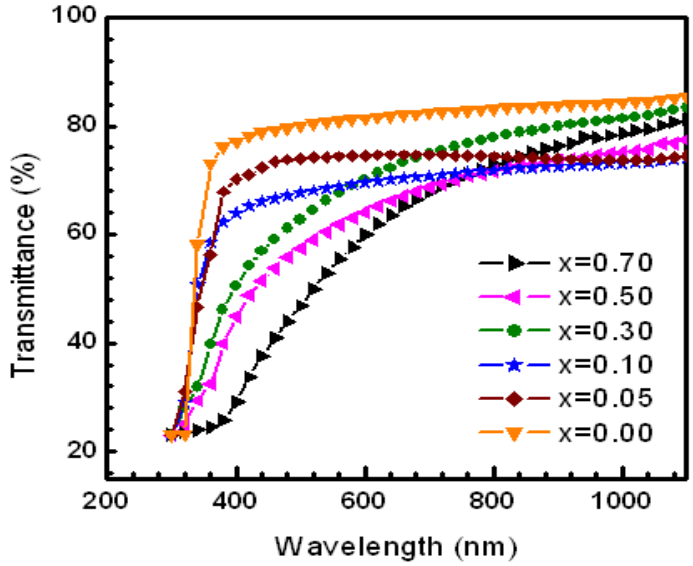

Fig. 4. wavelength vs. optical transmittance spectra of as deposited $Zn_{1-x}Mn_xS$ thin films

3.3 Optical band gap by τ relation

3.3.1 Direct band gap

The direct band gap energy of the films was calculated using the Tauc's relation $(\alpha h\nu)^2 = A(h\nu - E_g)$, Where A is a constant, α is the absorption coefficient, h is the Planck constant, υ is the frequency of the incident photon [30-31]. hν is photon energy. The optical band gap (E_g) is estimated from the plots of $(\alpha h\upsilon)^2$ vs. hυ for direct transition of undoped ZnS and Mn doped ZnS thin films by extrapolating straight lines on the energy axis. The band gap energies have been found about 3.51eV, 3.44 eV, 3.36 eV, 3.25 eV, and 3.01 eV of pure ZnS and $Zn_{1-x}Mn_xS$ thin films (x = 0.05, 0.10, 0.30, 0.50, and 0.70 mole) shown in Figure-5 which indicate the decrease of specific surface area and improved crystallinity nature of the films and are in good agreement with the other research works [19-20]. The nature of this variation in the band gap energy may be useful to design a suitable spintronic device.

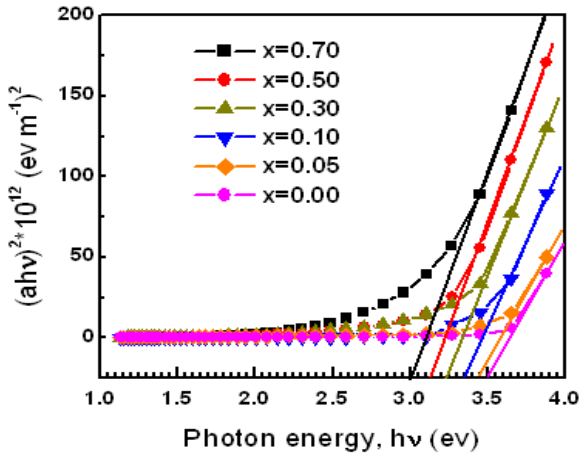

Fig. 5. Plots of $(\alpha h\nu)^2$ vs hν for direct transition

3.3.2 Indirect band gap

The value of indirect band gap energy is also calculated using the Tauc's relation

$$(\alpha h\nu)^{1/2} = A(h\nu - E_g)$$

The indirect band gap energies (Eg) of $Zn_{1-x}Mn_xS$ thin films have been carried out by extrapolating the linear region in the plot of $(\alpha h\nu)^{1/2}$ versus hν indicated decreasing tends from 3.02 eV to 1.85 eV shown in Figure-6. The energy gap for all transition is shown in Table-2 which satisfy the results reported by other researchers [22, 23]. This narrowing of band gaps lead to a redshift of the optical absorption. It is seen that both direct and indirect energy gap decreases slightly with increasing Mn doping concentration and direct band gap is higher than the indirect band gap energy. This may due to absorbing UV or Visible light by valance electrons which are promoted from ground state to exited state and have fixed values. On the other hand the causes of lower energy gap is for indirect transition of materials in the vibrational and rotational energy levels. The variation of direct and indirect band gap energy with Mn concentration are shown in Figure -7.

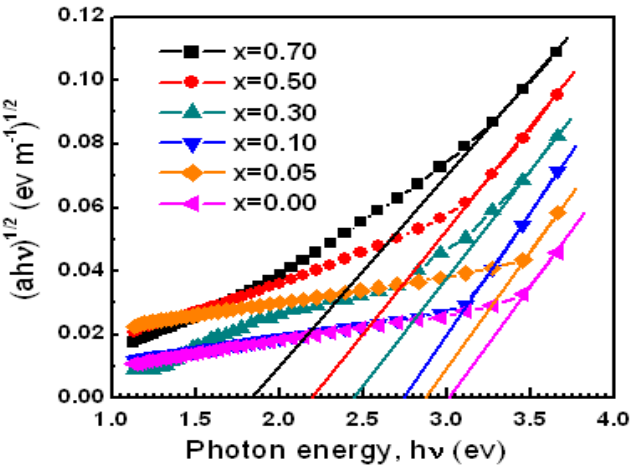

Fig. 6. Plots of $(\alpha h\upsilon)^{1/2}$ vs hν for indirect transition

Table-2 Direct and indirect band gap with Mn concentration

x(mole)	Eg (eV), Direct	Eg (eV), Indirect
0.00	3.51	3.02
0.05	3.44	2.88
0.10	3.36	2.74
0.30	3.25	2.45
0.50	3.14	2.21
0.70	3.01	1.85

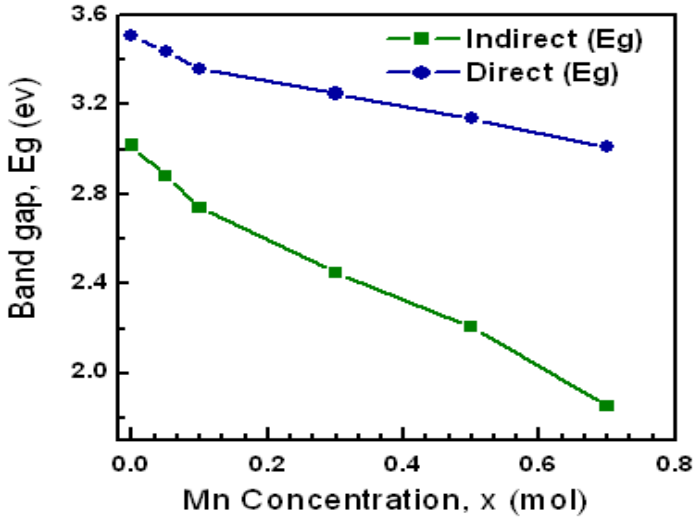

Fig.7. Variation of direct and indirect band gap energy with Mn concentration

3.4 Optical absorbance

Figure-8 shows the variation of absorbance (A) with wavelength (λ) for $Zn_{1-x}Mn_xS$ (x=0.00, 0.05, 0.10, 0.30, 0.50, 0.70 mole), films. It is seen that the absorbance values decrease with the increase in wavelength. In the visible and near infrared regions from 450 nm to 1100 nm low absorbance is observed.

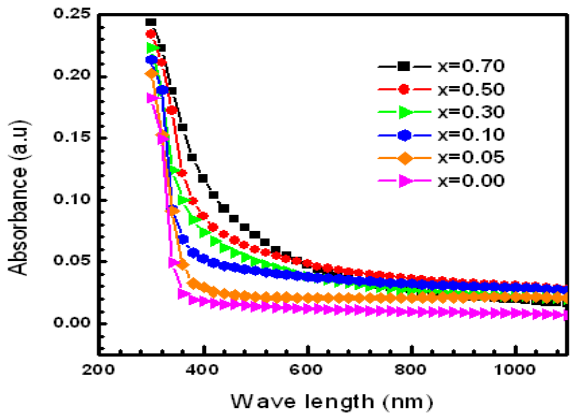

Fig. 8. Absorbance spectra of $Zn_{1-x}Mn_xS$ thin films

In the UV region absorption increases with the increasing incorporation of Mn. The enhanced absorption is observed in the neighborhood of λ= 400 nm. The sharp decreases in absorbance at the wavelength λ = 400 nm which may due to the onset of inter band transitions at the fundamental edge.

3.5 Reflectance

The reflectance (R) of $Zn_{1-x}Mn_xS$ (x=0.00, 0.05, 0.10, 0.30, 0.50, 0.70) thin films have been determined using the formula, R = 1 - (A + T); Where, A is absorbance and T is transmittance. The reflectance spectra with wave length is presented in Figure-9. The reflectance is small in the near infrared (NIR) and visible region. The overall reflectance of the films increase with increasing Mn concentration. [21].

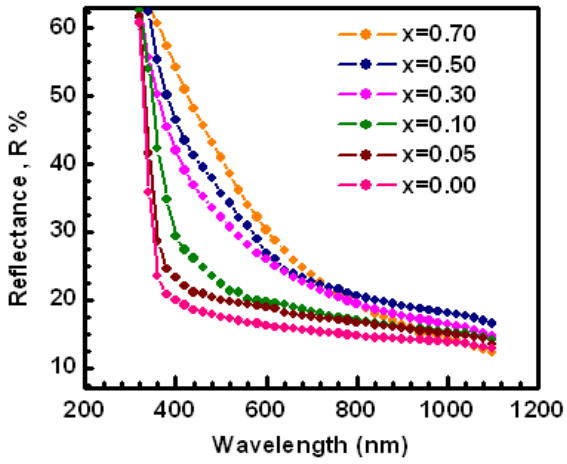

Fig. 9. Reflectance spectra of $Zn_{1-x}Mn_xS$ thin films

3.6 Extinction coefficient

The extinction coefficient (k) was obtained from the relation [22],

$$k = \frac{\alpha\lambda}{4\pi}$$

where λ is the wavelength, and α is absorption coefficient which are calculated from observed absorbance data using Beer Lambert's formula

$$\alpha = 2.303\left(\frac{A}{d}\right)$$

where A is the optical absorbance and d is the thickness of the film. The variation of extinction coefficient with photon energy is shown in Figure-10. The extinction coefficient increases with the increase of Mn incorporation. The rise and fall of extinction coefficients are due to the variation of absorbance. The fall in the extinction coefficient may be due to the absorption of light at the grain boundaries. From figure it is clear that k decreases rapidly with increasing wavelength from 300 nm to 400 nm and after that the value of k remains constant. The extinction coefficient is almost constant in the higher wavelength region.

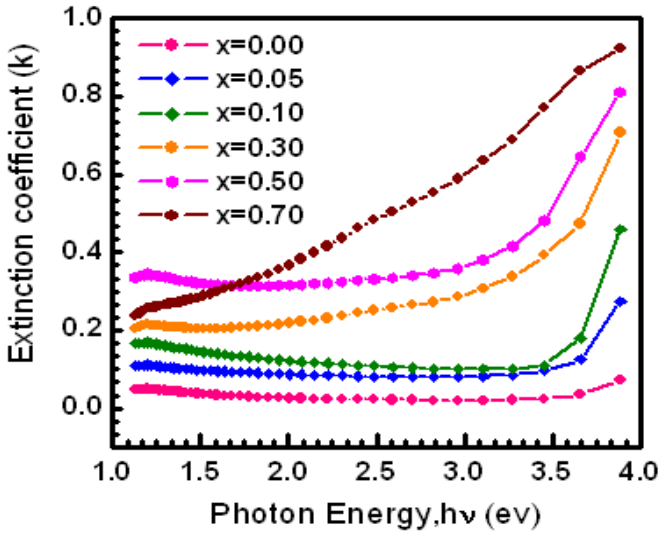

Fig. 10. Extinction coefficient of $Zn_{1-x}Mn_xS$ thin films

3.7 Refractive index

Figure-11 shows the variation of refractive index as a function of wavelength for $Zn_{1x}Mn_xS$ films of different Mn concentrations. The refractive index has been calculated using the relation

$$n = \left(\frac{1+R}{1-R}\right) + \sqrt{\left(\frac{4R}{(1-R)^2} - k^2\right)}$$

Where k is the extinction coefficient and R is the optical reflectance [22].

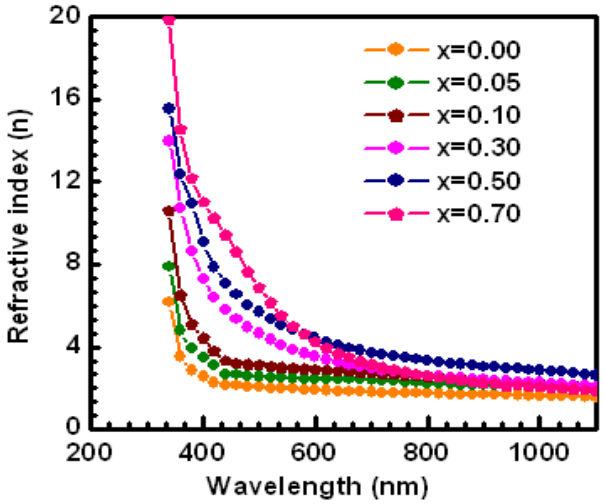

Fig. 11. Refractive index of $Zn_{1-x}Mn_xS$ as a function of wavelength

From the figure it is evident that the increase in the Mn incorpotion results in the overall increase in the refractive index which may due to the overall increase in the reflectance with the film thickness. Refractive index for pure ZnS was obtained 2.67 which is in good agreement with the value 2.62 reported by I. C. Ndukwe [23]. The variation of refractive index with wavelength at 700 nm for various Mn concentrations varies 3.33-4.67. The

gradual decrease of refractive index with wavelength implies that the normal dispersion occurred before the absorption edge followed by anomalous dispersion.

3.8 Dielectric constants

The real ε_r and imaginary ε_i parts of the dielectric constant were determined using the formula [24].

$\varepsilon_r = n^2 - k^2$, $\varepsilon_i = 2nk$.

The variation of real parts of the dielectric constant for different Mn concentrations are illustrated in Figure-12. The complex dielectric constant is fundamental intrinsic material property. The value of real parts of $Zn_{1-x}Mn_xS$ films varied between 3.8 to 8.2 indicating how much it will slow down the speed of light in the material. Figure-13 shows the variation of imaginary part of dielectric constants as a function of wavelength for $Zn_{1-x}Mn_xS$ films of different Mn concentrations. The value varied between 0.003 to 0.035. which gives that how a dielectric absorb energy from electric field due to dipole motion. The figures revealed that the values of the real part are higher than that of the imaginary part and follow the same pattern.

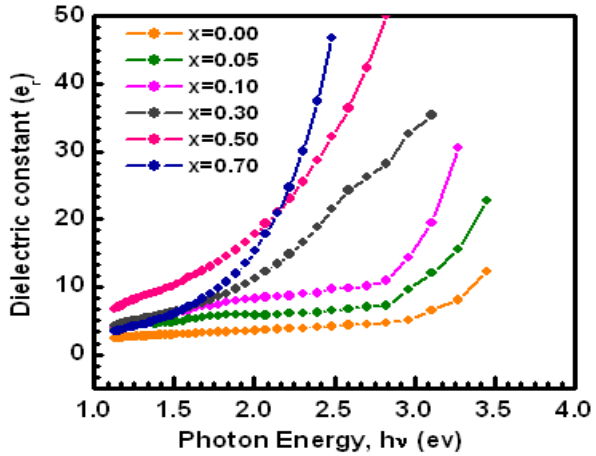

Fig. 12. Variation of real parts of dielectric constants of $Zn_{1-x}Mn_xS$

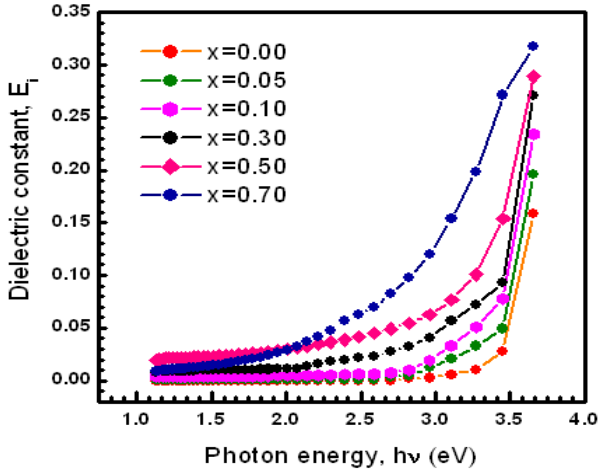

Fig. 13. Imaginary parts of dielectric constants of $Zn_{1-x}Mn_xS$

3.9 Dielectric loss

The variations of dielectric loss with photon energy are represented in Figure-14 for the as deposited $Zn_{1-x}Mn_xS$ thin films indicate a loss of energy that goes into heating a dielectric material in a varying electric field. The dielectric loss is given by, $\tan\delta = \varepsilon_2/\varepsilon_1$ and loss angle

$$\delta = \tan^{-1}\left(\frac{\varepsilon_2}{\varepsilon_1}\right)$$

where ε_1 and ε_2 are the real and imaginary parts of the dielectric constant [25]. From figure it is observed that dielectric loss decreases with high photon energies.

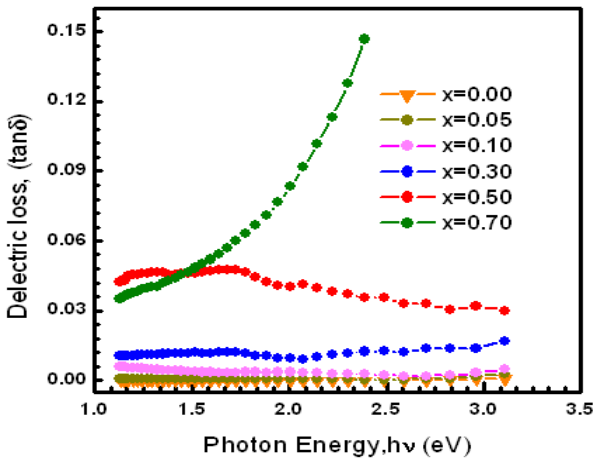

Fig. 14. Dielectric loss versus photon energy

3.10 Optical conductivity

Figure-15 shows the variation of optical conductivity with the incident photon energy. The optical conductivity has been determined using the relation $\sigma = \alpha nc/4\pi$; where c is the velocity of light [26] and observed he increased optical conductivity at high photon energies which is for high absorbance of thin films in that region.

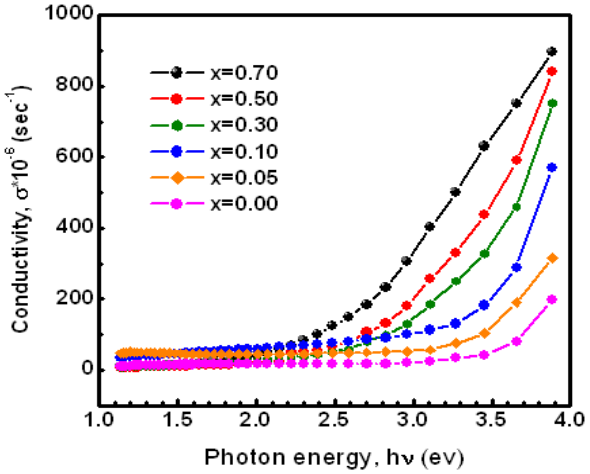

Fig. 15. Optical conductivity versus photon energy

4. Conclusions

In the present work, $Zn_{1-x}Mn_xS$ nanostructured DMS thin films have been prepared by a simple spray pyrolysis technique varying with Mn concentration at x = 0.00, 0.05, 0.10, 0.30, 0.50, 0.70 mole. FESEM micrographs showed nanostructured polycrystalline surface with 0.2 μm average crystallite size. The EADX analysis confirmed the presence of Mn^{2+} in $Zn_{1-x}Mn_xS$ matrix. More than 68% transmittances have been obtained at longer than 450 nm wavelengths. Direct band gaps are found from 3.01 eV to 3.51 eV and indirect band gaps from 1.85 eV to 3.02 eV in a decreasing trend indicating a red shift in the UV-Vis region which are in good agreement with the values reported by others. The refractive index is found 3.33-4.67. The reflectance, dielectric constant, and optical conductivity are also obtained in the increasing trend with Mn concentrations. The obtained values of these optical parameters indicated that $Zn_{1-x}Mn_xS$ film might be suitable for applications in the developments of spintronic devices.

Authorship contribution statement

Muslima Zahan: Investigation, Formal analysis, Methodology, Writing-original draft, Writing-review & editing, Conceptualization. **Krishna Pada Mondal:** Conceptualization, Visualization, Validation. **Jiban Podder:** Methodology, Formal analysis, Writing-review & editing, Supervision.

Declaration of competing interest

We certify that this manuscript has not yet been submitted to any journal and there are no affiliations with or involvement in any organization or entity with any financial interest that could have appeared to influence the work reported in this paper.

Data Availability

The data that support the findings of this study are available from the corresponding author upon reasonable request.

References

[1] Noor, N. A., Rashid, M., Mustafa,G. M., Mahmood, A., Al Masry, W., and Ramay, S. M., 2021, "Zinc based chalcogenides $ZnMn_2X_4$ (X= S, Se, Te) as promising spintronic and sustainable energy materials: Ab-initio DFT investigations," J. Alloys Compd., 856, pp. 157198.

[2] Ghosh, S., et al. 2022 "Transition metal ions in ZnS: A review on structure and properties," Mater. Today Proc., 62, pp. 1435-1440.

[3] Arora, A., and Singh, D., 2022, "Applications of II-VI semiconductors in optoelectronics," Mater. Sci. Eng. B, 234, pp. 153-170.

[4] Derbali A., Attaf A., Saidi H., Benamra H., Nouadji M., Aida M.S., Attaf N., Ezzaouia, H., 2018, "Investigaation of structural, optical and electrical properties of ZnS thin films prepared by ultrasonic spray technique for photovoltaic applications," Optik, 856, pp. 1-8.

[5] Bai, X., Wang, Y., and Fan. H., 2021, "Enhancement of photoluminescence properties of ZnS:Mn nanoparticles via thermal treatment," J. Alloys Compd., , 882: pp. 160938.

[6] Jrad, A., Naffouti,W., Nasr,T. B., Ammar,S., Turki-Kamoun,N., 2017, "Effect of manganese concentration on physical properties of ZnS: Mn thin films prepared by chemical bath deposition," J. Mater. Sci. Mater. Electron," 28, pp. 1463-1471.

[7] KantiKole,A., and Kumbhakar, P.,2012, "Cubic-to-hexagonal phase transition and optical properties of chemically synthesized ZnS nanocrystals," Result in physics, 2, pp. 150-155.

[8] Hernández-Fenollosa, M.A., López, M.C., Donderis, V., González, M., Marí, B., Ramos-Barrado, J.R., 2008, "Role of precursors on morphology and optical properties of ZnS thin films prepared by chemical spray pyrolysis," Thin solid films, 516, pp. 1622-1625.

[9] Kimi, M., Yuliati, L., and Shamsuddin, M., 2015, "Preparation of High Activity Ga and Cu Doped ZnS by Hydrothermal Method for Hydrogen Production under Visible Light Irradiation," J. of Nanomaterial, 5, pp. 1-9.

[10] Chandrasekar, L.B., Chandramohan, R., Vijayalakshmi, R., and Chandrasekaran, S., 2015, "Preparation and characterization of Mn-doped ZnS nanoparticles," Int Nano Lett, 5 pp. 71-75.

[11] Derbali, A., Attaf, A., Saidi, H., Aida, M., Benamra, H., Attaf, R., Attaf,N., and Ezzaouia, H., 2021, "Br doping effect on structural, optical and electrical properties of ZnS thin films deposited by ultrasonic spray," Mater. Sci. Eng., B., 268, pp. 115135.

[12] Maqsood, S., Javed, M. A., Mumtaz. S., and Al-Sadoon, M. K., 2024, "Computational study of Cd-based chalcogenide spinels $CdSm^2(S/Se)^4$ for spintronic applications, Chalcogenide Lett., 21(6), pp. 449–458.

[13] Wang, L., Ma, X., Chen, R., Yu, Y. Q., Luo, L. B., 2015, "Ultraviolet nano-photodetector based on ZnS: Cl nanoribbon/Au Schottky junctions," J. Mater. Sci. Mater. Electron., 26, pp. 4290-4297.

[14] Maqsood, S., Javed, M. A., Mumtaz. S., and Al-Sadoon, M. K., 2024, "Computational study of Cd-based chalcogenide spinels $CdSm^2(S/Se)^4$ for spintronic applications, Chalcogenide Lett., 21(6), pp. 449–458.

[15] Carranza, J., Luis, A., González, A., and Escorcia-García, J., 2025, "Luminescence enhancement of Mn2+-doped ZnS nanoparticles by insertion of Dy^{3+} ions", Ceramics Int., 51(25), pp. 46268-46276.

[16] Ravi, A, Cathrin Lims,S, and Sivakumar, M, 2024 "Tunable band gap energy of l-Cysteine-assisted formation of Mn-doped ZnS interconnected nanoparticles for electro-optic applications," Optical Materials, 150, , pp. 115293.

[17] Ali R. S., Rasheed H. S., Abdulameer N. D., Habubi N. F., and Chiad, S. S., 2023, "Physical properties of Mg doped ZnS thin films via spray pyrolysis," Chalcogenide Lett., 20(3), pp. 672-698.

[18] Aghaei, F., Sahraei, R., Soheyli, E., and Daneshfar, A., 2022, "Dopant-concentration dependent optical and structural properties of Cu-doped ZnS thin films," J. Nanostructures, vol. 12(2), pp. 330-342.

[19] Barman, B. and Sarma. K. C. 2020. "Low temperature chemical synthesis of ZnS, Mn doped ZnS nanosized particles: Their structural, morphological and photophysical properties," Solid State Sciences, 109, pp. 106404.

[20] Shobana, M., and Meher, S. R., 2019, "Effect of cobalt doping on the structural, optical and magnetic properties of sol gel derived ZnS nanocrystalline thin films and ab initio studies," Thin solid films, 683, pp. 97-110.

[21] Ahmed A. A., Aldaghri O., Salih E.Y., Ramizy A., Madkhali N., Alinad T., Ibnaouf K.H., and Eisaa, M. H. 2022, "Optical characteristics of Al-doped ZnS thin film using pulsed laser deposition technique: The effect of aluminium concentration." Chalcogenide Lett., 19(6), pp. 381-388.

[22] Torimoto, T., Obayashi, A., Kuwabata, S., Yasuda, H., Mori, H., and Yoneyama, H., 2000, "Preparation of size-quantized ZnS thin films using electrochemical atomic layer epitaxy and their photo electrochemical properties," Langmuir, 16, pp. 5820-5824.

[23] Hernandez, A., Medina-Velazquez, D. Y., Torre A. S., Morales-Ramirez, A., Molina-Morales, M., Barron-Meza, M. A., Ramírez-Quiros Y., and Reyes-Miranda, J., 2021, "Effect of europium on the blue–green emission of ZnS thin films by polyol and dip-coating technique," Mater. Sci. Semicond. Process., 121, pp. 105403.

[24] Poornima, N., Jose, A., Kartha, C. S., Vijayakumar, K., 2012, "Composition and Conductivity-type Analysis of Spray Pyrolysed ZnS Thin Films using Photoluminescence," Energy Procedia, 15, pp. 347-353.

[25] Ebrahimi, S., Yarmand, B., Naderi, N., 2019, "Enhanced optoelectrical properties of Mn-doped ZnS films deposited by spray pyrolysis for ultraviolet detection applications," Thin solid films, 676, pp. 31 41.

[26] Benamra, H., Saidi, V., Attaf, A., Aida, M., Derbali, A., and Attaf, N., 2020, "Physical properties of Al-doped ZnS thin films prepared by ultrasonic spray technique," Surf. Interfaces, 21, pp. 100645.

[27] Ghosh, S., et al., 2022, "Transition metal ions in ZnS: A review on structure and properties," Mater. Today Proc., 62, pp. 1435-1440.

[28]. Zahan, M., Islam, M. R., and Podder, J., 2019, "Influence of annealing temperature on tuning the band gap of Mn-doped ZnS thin films deposited by spray pyrolysis technique," Indian J Phys., 93 (5), pp. 611-616.

[29] Zahan, M., and Podder, j., 2019, "Surface morphology, optical properties and Urbach tail of spray deposited Co3O4 thin films," J Mater Sci: Mater Electron, 30 940, pp. 4259-4269

[30] Inamdar A. I., et al., 2016, "Optical properties in Mn-doped ZnS thin fi lms : Photoluminescence quenching," Mater. Lett., 163, pp. 126–129.

[31] Chakraborty, S., and Dasgupta. P., 2021, "Recent advancements in ZnS nanocrystal synthesis and applications," Mater. Today Chem., 19, pp. 100447.